Comparison of Direct and Spectral Methods for Evaluation of the Temperature Structure Parameter in Numerically Simulated Convective Boundary Layer Flows

JEREMY A. GIBBS

Department of Mechanical Engineering, University of Utah, Salt Lake City, Utah, and Cooperative Institute for Mesoscale Meteorological Studies, University of Oklahoma, Norman, Oklahoma

EVGENI FEDOROVICH

School of Meteorology, University of Oklahoma, Norman, Oklahoma

BJÖRN MARONGA

Institute of Meteorology and Climatology, Leibniz Universität Hannover, Hannover, Germany

CHARLOTTE WAINWRIGHT

School of Meteorology, University of Oklahoma, Norman, Oklahoma

MANUEL DRÖSE

Institute of Meteorology and Climatology, Leibniz Universität Hannover, Hannover, Germany

(Manuscript received 10 November 2015, in final form 17 February 2016)

ABSTRACT

In many engineering and meteorological applications, atmospheric turbulence within the planetary boundary layer is described in terms of its representative parameters. One such parameter is the structure-function (or structure) parameter that is used to characterize the intensity of turbulent fluctuations of atmospheric flow variables. Structure parameters are derivatives of structure functions, but are used more frequently than the latter ones for practical needs as they do not explicitly include dependence on the separation distance. The structure parameter of potential temperature, which is the subject of this study, describes the spatial variability of the temperature fluctuations. It is broadly represented in theories and models of electromagnetic and acoustic wave propagation in the atmosphere, and forms the basis for the scintillometer measurement concept. The authors consider three methods to compute the potential temperature structure function and structure parameter: the direct method, the true spectral method, and the conventional spectral method. Each method is tested on high-resolution potential temperature datasets generated from large-eddy simulations of a variety of convective boundary layer flow cases reproduced by two representative numerical codes. Results indicate that the popular conventional spectral method routinely exaggerates the potential temperature structure-function parameter, likely due to the unrealistic assumptions underlying the method. The direct method and true spectral method are recommended as the more suitable approaches.

1. Introduction

Knowledge of parameters of atmospheric turbulence within the planetary boundary layer is needed for many applications including pollutant dispersion modeling, wind engineering, weather forecasting, aviation, and prediction of electromagnetic and acoustic wave propagation. The latter group of applications, in particular, requires information on the so-called structure functions of the atmospheric flow fields that characterize turbulent fluctuations of atmospheric physical variables like air temperature or the refractive index of the air (Tatarskii 1961; Wyngaard et al. 1971; Wilson and Fedorovich 2012; Wainwright et al. 2015). From a statistical point of view, structure functions describe spatial variability of

Corresponding author address: Jeremy Gibbs, Department of Mechanical Engineering, University of Utah, 1495 E 100 S, 1550 MEK, Salt Lake City, UT 84112.
E-mail: jeremy.gibbs@utah.edu

DOI: 10.1175/MWR-D-15-0390.1

the chosen physical variable in relation to varying scales of its turbulent fluctuations. Usage of structure functions for quantification of turbulence dates back to the works of Kolmogorov (1941a,b) who established and described fundamental properties of turbulence dynamics and energy transformations in terms of velocity structure functions of different orders. In many applications and under certain assumptions, the structure functions are further distilled to structure-function (or simply, structure) parameters. These parameters are constant within the inertial subrange of the turbulence energy cascade and are designed to act as a singular descriptor of atmospheric turbulence under given conditions.

In this paper, we focus on structure functions and structure parameters of the potential temperature (hereafter called temperature for brevity) in the atmospheric convective boundary layer (CBL). This atmospheric boundary layer type is common for daytime fair-weather conditions over land and, given the dominance of large-scale (on the order of the layer depth) turbulent structures within the layer, is a popular object of numerical simulations.

Following the advent of the numerical large-eddy simulation (LES) technique (Lilly 1967), high-resolution LES have offered a robust source of data to study atmospheric turbulence in the CBL flows (Deardorff 1980; Fedorovich et al. 2004b; Maronga 2014). With respect to computation of the structure functions (of the second order) and structure parameters of a given physical variable from the gridded LES output, there are three methods commonly used in practice: the direct method (DM), the *true* spectral method (TSM), and the *conventional* spectral method (CSM). In the DM, the structure function is computed directly from the gridded field by using the mathematical definition of the function. Then, the structure parameter is evaluated by considering the structure function only for spatial scales that lie within the inertial subrange. Traditionally, the DM has been favored by the measurement community. According to the TSM, the structure function of a scalar is expressed through an integral form of the spectral density of the scalar (Tatarskii 1961; Wyngaard 2010). The beneficial trait of this method is that it reduces the computational overhead of the DM through the use of the numerically effective fast Fourier transform (FFT) technique to calculate the spectra. However, the TSM still involves numerical evaluation of the integrals, so the computational expense remains relatively high. Since this procedure is really just another form of the DM under the assumption of isotropy, it has not been widely adopted. Finally, by assuming that the entire scalar spectrum follows the inertial subrange form, the CSM employs an analytical relationship between the structure-function parameter and the spectral density of the scalar (Tatarskii 1961; Wyngaard et al. 1971). This relationship requires the least computational resources of the three methods, which has made it popular in practice (Wyngaard et al. 1971; Kaimal et al. 1976; Muschinski et al. 2004; Maronga et al. 2013; Maronga 2014; Maronga et al. 2014). While the CSM has been employed in observational studies using fast sensors, it has recently proven popular also among numerical modelers since spectra are easily computed from three-dimensional output.

In the present study, we numerically analyze output data from two contemporary LES codes to examine performance of the considered three methods applied to evaluate structure functions and parameters of temperature in a variety of CBL flow types and to offer recommendations on their use. We believe this to be important because the use of high-resolution simulations for study of atmospheric turbulence properties is becoming more popular. Thus, we hope to further investigate the procedures of structure function and structure parameter retrieval from numerical data by showing which method gives the best trade-off of accuracy and computational burden. To our knowledge, such a comparison has not been described in the literature. By using two numerical codes with differing setups, we aim to minimize any concerns regarding dependence of the conclusions on the employed numerical technique, initialization settings, or forcing mechanism.

Mathematical details of the structure function and structure parameter calculation with the three evaluated methods are given in section 2. The employed LES codes, simulated CBL flow types, and data processing techniques are discussed in section 3. The results are presented in section 4. Finally, section 5 contains a discussion and conclusions of our investigation.

2. Structure function and structure-function parameter formulations

Spatial variability of temperature fluctuations associated with atmospheric turbulence is typically described in terms of the second-order temperature structure function (Tatarskii 1961; Wyngaard 2010), given by

$$\overline{(\delta\theta)^2}(\mathbf{r},t) = \overline{[\theta(\mathbf{x},t) - \theta(\mathbf{x}+\mathbf{r},t)]^2}, \tag{1}$$

where θ is potential temperature, $\mathbf{x}$ is a position vector, $\mathbf{r}$ is a separation vector, t is time, and overbars represent the ensemble average. If the separation distance $r = |\mathbf{r}|$ lies within the inertial subrange of spatial scales of turbulent temperature fluctuations, and the turbulence is

assumed locally isotropic, then the temperature structure function may be expressed as

$$\overline{(\delta\theta)^2} = C_\theta^2 r^{2/3}, \tag{2}$$

where C_θ^2 is the temperature structure-function parameter, often just called the temperature structure parameter (the absolute temperature T is often considered in the literature instead of θ). Approximating ensemble averaging in Eqs. (1) and (2) by spatial averaging over statistically homogeneous directions (typically taken along horizontal lines or planes) and adopting the assumption of turbulence isotropy, one may apply Eq. (1) to directly compute the temperature structure function from gridded LES data, identify the inertial subrange of r within the entire domain of the computed function, and then normalize the inertial-subrange values of the function by $r^{2/3}$ using Eq. (2) to obtain the structure parameter. Implementation of this procedure (hereafter referred to as DM) for post-processing of the LES CBL data is described in Wilson and Fedorovich (2012) and Wainwright et al. (2015). Computationally, however, DM is relatively expensive. Another issue is that experimentally the DM requires measurements over different separation distances, which means multiple observational points. While the DM may be applied to evaluate structure functions from high-frequency time series data using Taylor's frozen turbulence hypothesis, its general applicability to measured heterogeneous flow fields would still be limited. Accordingly, more computationally and conceptually affordable methods were historically sought for physically appropriate evaluation of the structure parameter from observational and numerical simulation data.

A group of such methods is based on the relation between $\overline{(\delta\theta)^2}$ and one-dimensional spectral density of temperature Φ_θ applicable in isotropic turbulence (Tatarskii 1961; Wyngaard 2010):

$$\overline{(\delta\theta)^2} = 4\int_0^\infty [1-\cos(kr)]\Phi_\theta(k)\,dk, \tag{3}$$

where k is wavenumber. Importantly, in the above expression no assumption is made about the particular form of the spectral density function under the integral. Since the gridded temperature fields over horizontal planes are available from the LES data, the temperature structure function and structure parameter are readily evaluated using Eqs. (3) and (2). We call this approach TSM. Since the numerical FFT technique allows for relatively fast computation of Φ_θ, the TSM is potentially faster than the DM. However, the combined requirements of computing the spectral density and the integral in Eq. (3) make TSM still a relatively expensive procedure.

If Φ_θ is assumed to have the inertial-subrange form $\propto k^{-5/3}$ within the entire interval of turbulence scales in Eq. (3), then the integral on the right-hand side may be calculated analytically (Tatarskii 1961; Essenwanger and Reiter 1969; Wyngaard et al. 1971) and used in combination with Eq. (2) to obtain

$$\Phi_\theta(k) = \frac{2\Gamma(5/3)}{2\pi}\sin\left(\frac{\pi}{3}\right)C_\theta^2 k^{-5/3}, \tag{4}$$

where Γ is the gamma function. Rearrangement and approximation of Eq. (4) yields

$$C_\theta^2 \approx \frac{\Phi_\theta(k)}{0.25\,k^{-5/3}}. \tag{5}$$

We call the above method of the C_θ^2 evaluation the CSM. Since in this case the evaluation of C_θ^2 requires only computation of the one-dimensional spectral density, the CSM remains a popular technique in numerical modeling studies for calculation of structure parameters of different physical variables in atmospheric flows. Additionally, the CSM makes the turbulence spectrum of a scalar analytically tractable. Experimentally, the CSM has been a popular choice since it may be applied to point observations with fast sensors. The inertial subrange in turbulent fluctuations detected by these sensors often extends toward the smallest observable scale, meaning that the method is less susceptible to deviations from the Kolmogorov $-5/3$ slope.

3. Large-eddy simulation data

a. OU-LES

The University of Oklahoma LES code (OU-LES; Fedorovich et al. 2001, 2004b) stems from the Delft University LES code (Nieuwstadt 1990), from which several other modern LES codes are also derived [e.g., the Dutch Atmospheric Large-Eddy Simulation (DALES); Heus et al. 2010]. The OU-LES code numerically solves the filtered Boussinesq-approximated Navier–Stokes equations of motion and the scalar transport equations. Advection/convection terms in the equations are approximated using second-order, centered finite differences. Time integration of the equations is carried out by a third-order Runge–Kutta scheme, as in Sullivan et al. (1996). The subgrid turbulence closure is a version of the Deardorff (1980) closure model based on the parameterized transport equation for the subgrid turbulence kinetic energy. The ability of the OU-LES code to reproduce the shear-free CBL was assessed in

TABLE 1. Simulation configuration values for geostrophic wind (u_g; v_g was always zero), surface kinematic heat flux ($\overline{w'\theta'}$), surface kinematic moisture flux ($\overline{w'q'}$), surface roughness (z_0), horizontal (Δh) and vertical (Δz) grid spacing, and numerical mesh size ($N_x \times N_y \times N_z$).

Code	Case	u_g (m s^{-1})	$\overline{w'\theta'}$ (K m s^{-1})	$\overline{w'q'}$ (m s^{-1})	z_0 (m)	Δh (m)	Δz (m)	$N_x \times N_y \times N_z$
OU-LES	Free	0	0.12	5×10^{-5}	0.14	10	10	$512 \times 512 \times 200$
	Shear	10						
PALM	Free	0	0.075	1.1×10^{-4}	0.10	4	2	$2016 \times 2016 \times 1008$
	Shear	6						

Fedorovich et al. (2004a) through comparisons with bulk models and water tank data. Its applicability to the shear-driven CBL was investigated and verified in Fedorovich et al. (2001). Finally, adherence of the simulated velocity fields to fundamental laws of turbulence spectral behavior was studied in Gibbs and Fedorovich (2014) for both shear-free and shear-driven CBL flows.

b. PALM

The Parallelized Large-Eddy Simulation Model (PALM; Raasch and Schröter 2001; Maronga et al. 2015) is a descendant of the nonparallelized LES code developed by Raasch and Etling (1991). The PALM code operates with filtered, Boussinesq-approximated Navier–Stokes equations. The advection/convection terms are discretized using upwind-biased fifth-order finite differences, while time integration is achieved using a third-order Runge–Kutta scheme following Williamson (1980). Similar to the OU-LES code, subgrid terms are modeled using the approach of Deardorff (1980). In addition, PALM offers numerous supplementary advanced features, such as a coupled ocean model, and embedded microphysics, particle transport, cloud, and canopy models. PALM has been successfully applied to simulate various boundary layer regimes, including the homogeneously heated CBL (e.g., Raasch and Franke 2011; Maronga et al. 2013), the heterogeneously heated CBL (e.g., Maronga and Raasch 2013), urban canopy flows (Kanda et al. 2013), and cloudy boundary layers (e.g., Heinze et al. 2015; Hoffmann et al. 2015).

c. Investigated CBL flow types

The three methods—DM, TSM, and CSM—were tested using data from simulations of different shear-free and shear-driven CBLs. Details for each simulation configuration are given in Table 1. Both codes enforced Monin–Obukhov flux–profile relationships (Monin and Obukhov 1954) locally within the near-surface layer of grid cells to relate dynamic and thermal properties of the flow. Additionally, every simulation applied Rayleigh damping in the upper portion of the domain and used periodic lateral boundary conditions. In each case, idealized well-mixed profiles of virtual potential temperature and moisture with an overlying capping inversion were used to initialize simulations for both CBL flow types. Settings and procedures generally followed those in the originating publications referenced below. The evaluation of each method on data generated by differing codes with individual simulation configurations was carried out to improve the robustness of our conclusions.

For OU-LES, the simulations were set up as in Gibbs and Fedorovich (2014), with the exception of a refined grid spacing. Simulations lasted 12 h and three-dimensional simulated flow fields for testing of the three methods were extracted at the midpoint of the final hour of the simulation. PALM simulations followed the setup of the W00 and W06 cases denoted in Maronga (2014), which were based on simulations described in Maronga et al. (2013), with the exception of a modified numerical grid size. Vertical grid stretching was applied in the free atmosphere, well above the CBL top, in order to optimize computational expense. Flow field data were extracted after 1 h of simulation time.

Horizontal [OU-LES (Figs. 1a1; 2a1); PALM (Figs. 1b1; 2b1)] and vertical [OU-LES (Figs. 1a2; 2a2); PALM (Figs. 1b2; 2b2)] cross sections of the extracted potential temperature fields are shown for the shear-free and shear-driven cases in Figs. 1 and 2, respectively. In the shear-free cases, both codes reproduce the expected traditional cellular-type convection patterns, although PALM structures appear slightly more organized. Elongated structures associated with the imposed mean wind are evident for both codes in the shear-driven cases, although those reproduced by OU-LES are apparently more coherent and affected by the Coriolis force due to the stronger flow. For both sheared and shear-free flow types, OU-LES generates a slightly deeper boundary layer. This feature is likely due to the combined effects of stronger surface forcing, coarser resolution, and smaller domain size.

d. Data processing

Single three-dimensional potential temperature fields from the OU-LES and PALM simulation datasets

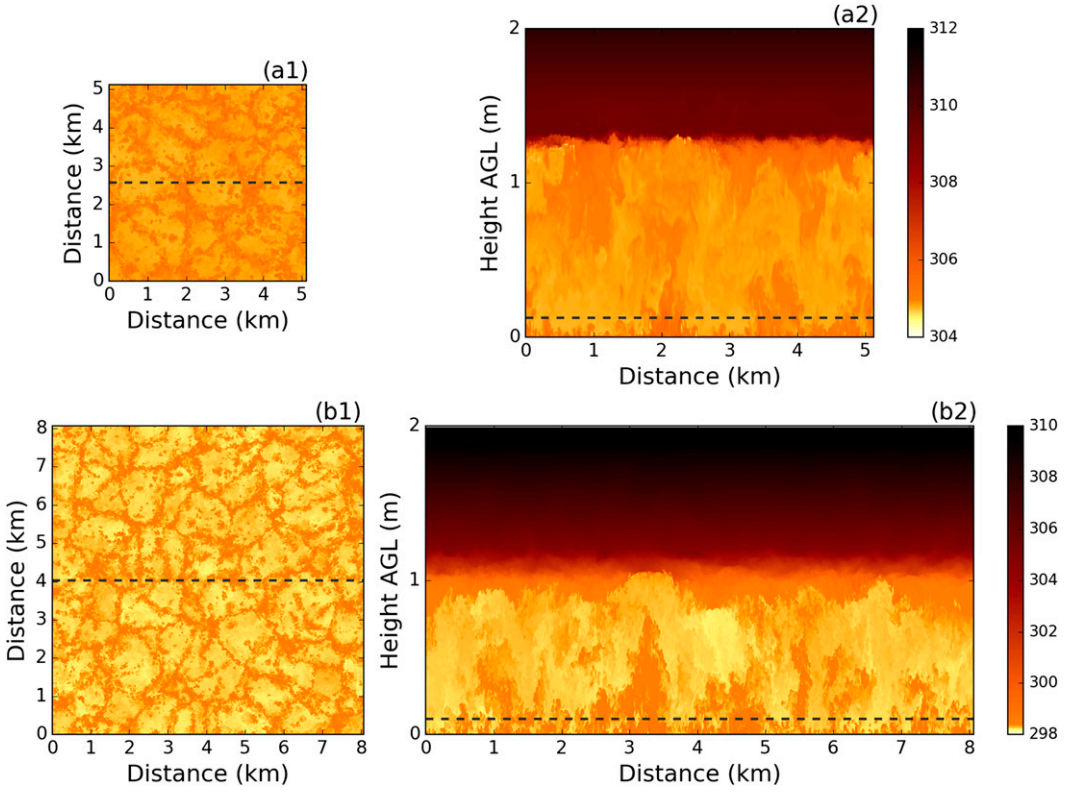

FIG. 1. Potential temperature reproduced by (a1),(a2) OU-LES and (b1),(b2) PALM for the shear-free CBL case. (a1),(b1) Horizontal cross sections are taken at $z/z_i = 0.1$, where z_i is the depth of the boundary layer, and (a2),(b2) x–z vertical cross sections are taken at the midpoint in the y direction. Cross-sectional locations are denoted by dashed black lines.

described in section 3c were used to evaluate the three-structure parameter computation methods. Individual snapshots were used because there were no significant temporal variations in the structure parameters after the simulations reached a quasi-stationary state. When implementing the DM, structure functions were computed following the procedures outlined in Wilson and Fedorovich (2012) and Wainwright et al. (2015). Within each horizontal plane, squared temperature differences were summed along each row in the x direction for a given separation distance using Eq. (1). Once summed, the planar mean value of squared temperature difference was computed and the process was repeated for each separation distance. As a first step of the TSM and CSM implementation, the one-dimensional spectral density (spectra) of potential temperature was computed following the algorithm described in Gibbs and Fedorovich (2014). For a given horizontal cross section, potential temperature spectra were calculated along every row in the x direction and subsequently averaged over the y direction. The procedure was repeated for each height. By computing the potential temperature structure functions and spectra in this manner, turbulence was implicitly assumed to be isotropic over horizontal planes, and both evaluated statistics were affected by the existing temperature-field anisotropy in a similar fashion. The inertial subranges in spectra needed for the CSM implementation were identified at each height procedurally [similarly to the method suggested by Hartogensis and De Bruin (2005)] as the largest contiguous regions of wavenumbers over which the spectral density followed the $-5/3$ power law, within a relative error allowance of 30% and a root-mean-square error tolerance of 15%. Inertial intervals of separation distances in structure functions (DM case) were obtained in analogous manner but using the 2/3 power-law criterion. Since spectral density is generally noisy, a Hanning-type smoother (Press et al. 1986) was applied to each spectrum before identifying the inertial subrange in the CSM. The representative inertial subrange values of wavenumber k and separation distance r were taken as the geometric mean of k and the geometric mean of r within the identified inertial intervals. Since these methods strongly rely on the inertial-subrange identification procedure, the objectively determined inertial subranges were checked visually for accuracy and

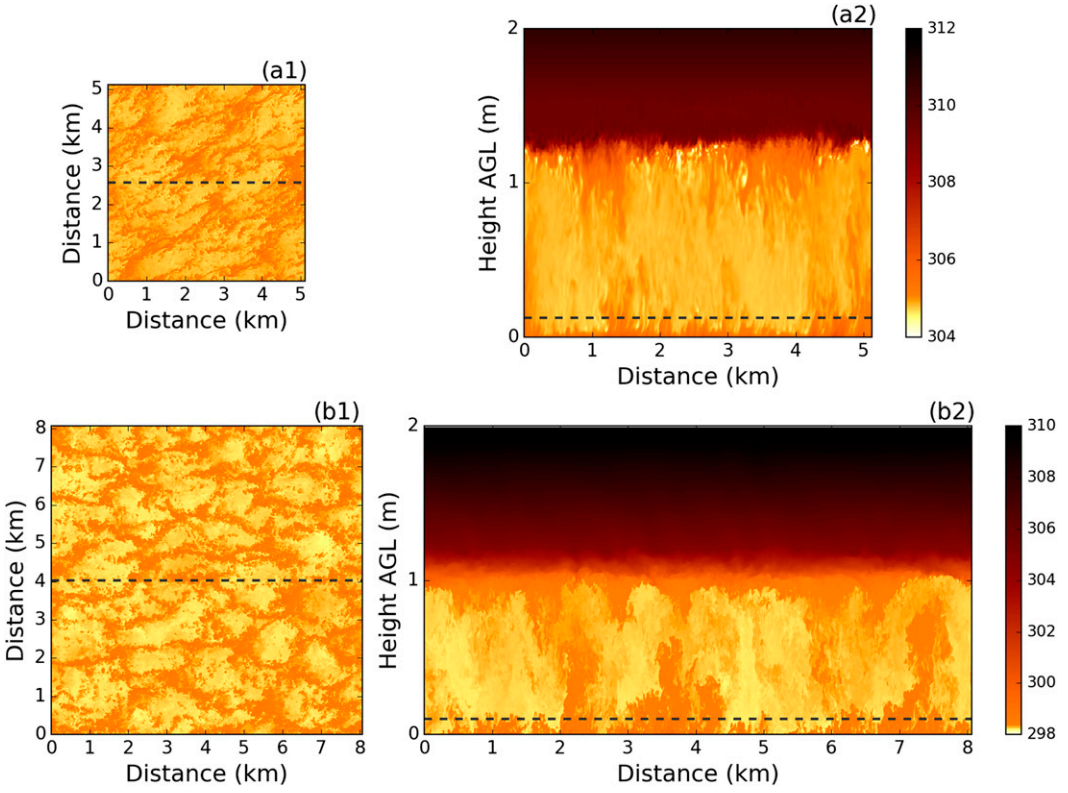

FIG. 2. As in Fig. 1, but for the shear-driven CBL case.

consistency. The procedural method applied to the shear-free case reproduced by OU-LES at height $z/z_i = 0.5$, where z_i is the depth of the boundary layer, is illustrated in Fig. 3. Following the TSM approach, the computed one-dimensional spectra were integrated using Eq. (3) to obtain structure functions. These structure functions were objectively analyzed to identify inertial subranges of r in the same way as in the DM case. Using obtained k and

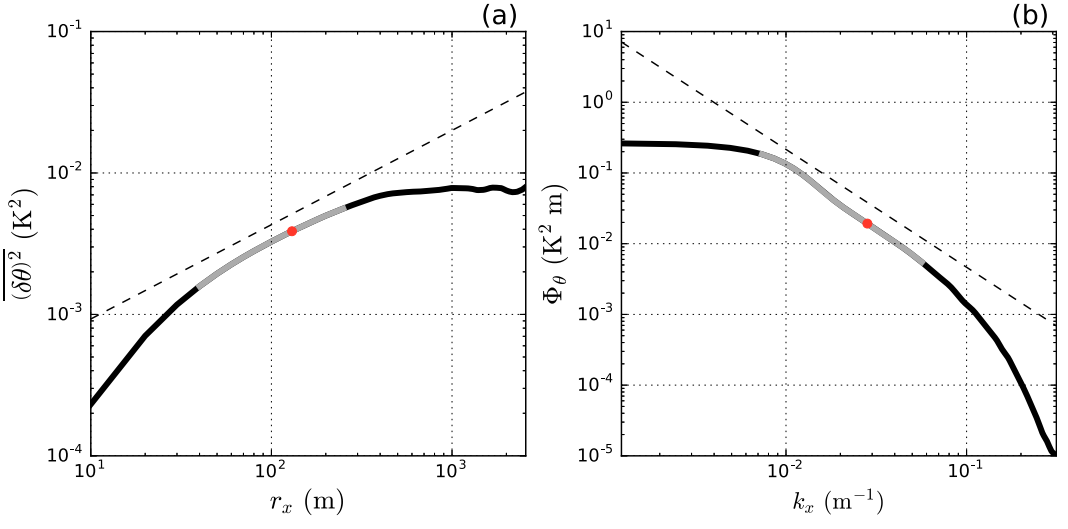

FIG. 3. (a) Structure function and (b) one-dimensional spectral density of potential temperature in the x direction at $z/z_i = 0.5$, where z_i is the depth of the boundary layer, for the shear-free case reproduced by OU-LES. Black lines are the respective quantities, gray lines show the objectively identified inertial subranges, and red dots are the geometric mean values within the inertial subrange that are used for the respective calculations.

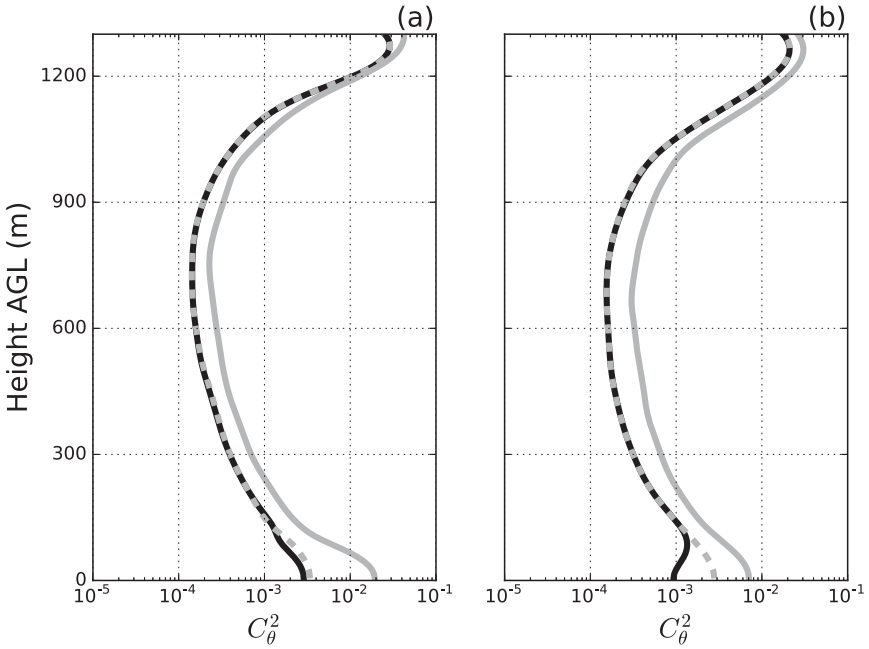

FIG. 4. Vertical profiles of C_θ^2 computed from OU-LES data using the direct method (DM; solid black), the true spectral method (TSM; dashed gray), and the conventional spectral method (CSM; solid gray) for the (a) shear-free and (b) shear-driven CBL cases.

r values, structure parameters were evaluated from Eq. (2) (DM and TSM cases) and from Eq. (5) (CSM case). In all cases, confidence intervals were computed in order to examine the uncertainty of each structure-function profile. At each height, the standard deviation was computed across the inertial subrange and divided by the square root of sample size. Owing to the relatively wide inertial subrange and ample number of rows used for each respective averaging procedure, the effective sample size was quite large. Since structure parameter values did not vary that greatly within the inertial subrange, the standard deviations were relatively small. As a result, the standard error values were one to two orders of magnitude smaller than the corresponding structure parameter values. Accordingly, we omitted their inclusion in Figs. 4 and 5.

4. Results

Based on the procedures outlined in section 3d, individual vertical profiles of C_θ^2 obtained by DM, TSM, and CSM were constructed. Profiles for the shear-free and shear-driven CBL flows simulated with OU-LES and PALM codes are shown in Figs. 4 and 5, respectively. One may readily notice that the OU-LES and PALM profiles share the same overall behavior, but in details they differ. For instance, the near-surface values from OU-LES seem to cut off and approach constant values as compared to those from the PALM data. This may be a result of the combined effects of the coarser resolution and less accurate numerics used in OU-LES. It is also readily apparent that the CSM values of C_θ^2 are consistently larger than those from the DM and TSM, which very closely overlap one another. The CSM values are approximately twice as large at the top of the CBL, around 3 times as large in the middle portion of the CBL, and as much as an order-of-magnitude larger than DM and TSM values near the surface. The DM procedure may be considered the most relevant and reliable of the three since it closely corresponds to the mathematical definition of the structure function. Accordingly, the observed behavior points to a persistent overestimation of the C_θ^2 by CSM, which is found in simulation data for two CBL flow types being simulated by two different LES codes employed with different numerical domain sizes, and different grid spacings and surface forcings.

5. Discussion and conclusions

The comparison results presented here are somewhat surprising given the historical popularity of the CSM. In fact, a recent study found good agreement between C_T^2 computed using DM and CSM applied to aircraft and large-aperture scintillometer (LAS) data (Braam et al. 2016). This agreement may result from the previously

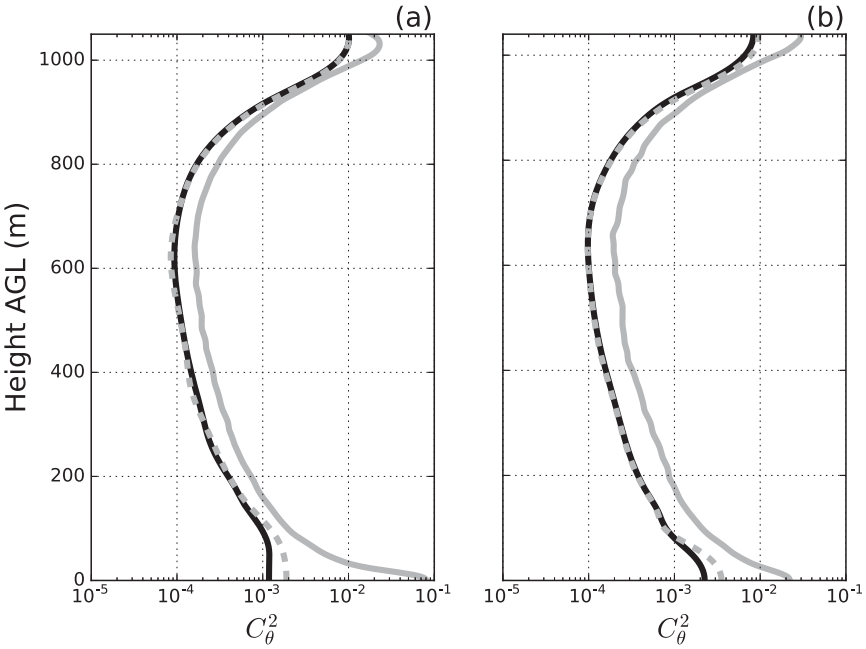

FIG. 5. As in Fig. 4, but computed from PALM data.

discussed benefits of applying the CSM to local point observations using fast sensors. In another example, Maronga et al. (2013) compared C_T^2 calculated using the CSM on aircraft and LAS data with profiles derived from LES data using the same method. They found good agreement in the case of the LAS data and acceptable agreement in the case of aircraft data. However, there is some measure of support in the recent literature for the findings presented in this study. Maronga et al. (2014), using the same method, found overestimation of C_T^2 computed from LES data compared with data from a LAS.

We suspect that the observed differences in values for C_θ^2 between the TSM and CSM are the result of assumptions used to arrive at Eq. (5). Recall that for the relationship described by Eq. (3), there are no restrictions placed on the employed temperature spectrum. However, while applying this equation to arrive at the approximate expression given by Eq. (5), it is assumed that the entire temperature spectrum follows the inertial subrange $-5/3$ power law, which is rather unrealistic. Obviously, the realistic atmospheric spectrum for temperature would follow this power law only within a certain range of k. While the TSM implicitly allows for the inclusion of the spectral regions beyond the inertial subrange, their omission in the CSM results in an overprediction of C_θ^2. This exaggeration is most visible in the near-wall region where the effect is additionally modulated by the turbulence anisotropy over the (x, y) planes. Note that the DM and TSM profiles also differ in this region. This is apparently another manifestation of turbulence anisotropy over horizontal planes that differently affects evaluation of structure parameters by these two methods.

The reduction of the temperature structure parameter calculation to a simple formula relating this parameter to one-dimensional spectral density in the inertial subrange (the CSM) was apparently a result of feasible computational simplification that was motivated, at least partially, by the limited computational resources available at the time when the method was conceived. Another attractive feature of the CSM is its applicability to point observations. In light of the results presented herein, and the relative abundance of modern computing power, we cannot recommend the continued employment of Eq. (5) for numerical evaluation of structure parameters. While we believe that contemporary computer resources can readily handle the DM, we suggest that if a reduction in computation effort is required, then the TSM should be used.

Acknowledgments. The authors thank Heather Grams, Ryan May, Ryan Sobash, Zac Flamig, Patrick Marsh, James Correia Jr., David J. Gagne II, Tim Supinie, Kevin Manross, Benjamin Root, and Kelton Halbert for their helpful suggestions regarding aspects of data post-processing methods used in this study. Conversations with Alan Shapiro (University of Oklahoma) and Arnold

Moene (Wageningen University) were especially insightful. PALM simulations were performed on the Cray XC 30 at The North-German Supercomputing Alliance (HLRN), Hannover/Berlin, Germany.

REFERENCES

Braam, M., F. Beyrich, J. Bange, A. Platis, S. Martin, B. Maronga, and A. F. Moene, 2016: On the discrepancy in simultaneous observations of the structure parameter of temperature using scintillometers and unmanned aircraft. *Bound.-Layer Meteor.*, **158**, 257–283, doi:10.1007/s10546-015-0086-9.

Deardorff, J. W., 1980: Stratocumulus-capped mixed layers derived from a three-dimensional model. *Bound.-Layer Meteor.*, **18**, 495–527, doi:10.1007/BF00119502.

Essenwanger, O., and E. R. Reiter, 1969: Power spectrum, structure function, vertical wind shear, and turbulence in troposphere and stratosphere. *Arch. Meteor. Geophys. Bioklimatol.*, **18A**, 17–24, doi:10.1007/BF02247861.

Fedorovich, E., R. Conzemius, and D. Mironov, 2004a: Convective entrainment into a shear-free linearly stratified atmosphere: Bulk models reevaluated through large eddy simulations. *J. Atmos. Sci.*, **61**, 281–295, doi:10.1175/1520-0469(2004)061<0281:CEIASL>2.0.CO;2.

——, and Coauthors, 2004b: Entrainment into sheared convective boundary layers as predicted by different large eddy simulation codes. *16th Symp. on Boundary Layers and Turbulence*, Portland, ME, Amer. Meteor. Soc., P4.7. [Available online at https://ams.confex.com/ams/BLTAIRSE/techprogram/paper_78656.htm.]

——, F. T. M. Nieuwstadt, and R. Kaiser, 2001: Numerical and laboratory study of horizontally evolving convective boundary layer. Part I: Transition regimes and development of the mixed layer. *J. Atmos. Sci.*, **58**, 70–86, doi:10.1175/1520-0469(2001)058<0070:NALSOA>2.0.CO;2.

Gibbs, J. A., and E. Fedorovich, 2014: Comparison of convective boundary layer velocity spectra retrieved from large-eddy-simulation and Weather Research and Forecasting Model data. *J. Appl. Meteor. Climatol.*, **53**, 377–394, doi:10.1175/JAMC-D-13-033.1.

Hartogensis, O. K., and H. A. R. De Bruin, 2005: Monin–Obukhov similarity functions of the structure parameter of temperature and turbulent kinetic energy dissipation rate in the stable boundary layer. *Bound.-Layer Meteor.*, **116**, 253–276, doi:10.1007/s10546-004-2817-1.

Heinze, R., D. Mironov, and S. Raasch, 2015: Second-moment budgets in cloud-topped boundary layers: A large-eddy simulation study. *J. Adv. Model. Earth Syst.*, **7**, 510–536, doi:10.1002/2014MS000376.

Heus, T., and Coauthors, 2010: Formulation of the Dutch Atmospheric Large-Eddy Simulation (DALES) and overview of its applications. *Geosci. Model Dev.*, **3**, 415–444, doi:10.5194/gmd-3-415-2010.

Hoffmann, F., S. Raasch, and Y. Noh, 2015: Entrainment of aerosols and their activation in a shallow cumulus cloud studied with a coupled LCM-LES approach. *Atmos. Res.*, **156**, 43–57, doi:10.1016/j.atmosres.2014.12.008.

Kaimal, J. C., J. C. Wyngaard, D. A. Haugen, O. R. Coté, and Y. Izumi, 1976: Turbulence structure in the convective boundary layer. *J. Atmos. Sci.*, **33**, 2152–2169, doi:10.1175/1520-0469(1976)033<2152:TSITCB>2.0.CO;2.

Kanda, M., A. Inagaki, T. Miyamoto, M. Gryschka, and S. Raasch, 2013: A new aerodynamic parameterization for real urban surfaces. *Bound.-Layer Meteor.*, **148**, 357–377, doi:10.1007/s10546-013-9818-x.

Kolmogorov, A., 1941a: The local structure of turbulence in incompressible viscous fluid for very large Reynolds' numbers. *Dokl. Akad. Nauk SSSR*, **30**, 301–305.

——, 1941b: Dissipation of energy in locally isotropic turbulence. *Dokl. Akad. Nauk SSSR*, **32**, 16–18.

Lilly, D. K., 1967: The representation of small-scale turbulence in numerical simulations. *Proc. IBM Scientific Computing Symp. on Environmental Sciences*, IBM Form 320-1951, Yorktown Heights, NY, IBM, 195–209, doi:10.5065/D62R3PMM.

Maronga, B., 2014: Monin–Obukhov similarity functions for the structure parameters of temperature and humidity in the unstable surface layer: Results from high-resolution large-eddy simulations. *J. Atmos. Sci.*, **71**, 716–733, doi:10.1175/JAS-D-13-0135.1.

——, and S. Raasch, 2013: Large-eddy simulations of surface heterogeneity effects on the convective boundary layer during the LITFASS-2003 experiment. *Bound.-Layer Meteor.*, **146**, 17–44, doi:10.1007/s10546-012-9748-z.

——, A. F. Moene, D. van Dinther, S. Raasch, F. C. Bosveld, and B. Gioli, 2013: Derivation of structure parameters of temperature and humidity in the convective boundary layer from large-eddy simulations and implications for the interpretation of scintillometer observations. *Bound.-Layer Meteor.*, **148**, 1–30, doi:10.1007/s10546-013-9801-6.

——, O. Hartogensis, S. Raasch, and F. Beyrich, 2014: The effect of surface heterogeneity on the structure parameters of temperature and specific humidity: A large-eddy simulation case study for the LITFASS-2003 experiment. *Bound.-Layer Meteor.*, **153**, 441–470, doi:10.1007/s10546-014-9955-x.

——, and Coauthors, 2015: The Parallelized Large-Eddy Simulation Model (PALM) version 4.0 for atmospheric and oceanic flows: Model formulation, recent developments, and future perspectives. *Geosci. Model Dev.*, **8**, 2515–2551, doi:10.5194/gmd-8-2515-2015.

Monin, A. S., and A. M. Obukhov, 1954: Basic laws of turbulent mixing in the surface layer of the atmosphere. *Tr. Akad. Nauk. SSSR Geophiz. Inst.*, **24** (151), 163–187.

Muschinski, A., R. G. Frehlich, and B. B. Balsley, 2004: Small-scale and large-scale intermittency in the nocturnal boundary layer and the residual layer. *J. Fluid Mech.*, **515**, 319–351, doi:10.1017/S0022112004000412.

Nieuwstadt, F. T. M., 1990: Direct and large-eddy simulation of free convection. *Proc. Ninth Int. Heat Transfer Conf.*, Jerusalem, Israel, American Society of Mechanical Engineers, 37–47.

Press, W. H., B. Flannery, S. Teukolsky, and W. Vetterling, 1986: *Numerical Recipes: The Art of Scientific Computing.* Cambridge University Press, 818 pp.

Raasch, S., and D. Etling, 1991: Numerical simulation of rotating turbulent thermal convection. *Beitr. Phys. Atmos.*, **64**, 185–189.

——, and M. Schröter, 2001: PALM—A large-eddy simulation model performing on massively parallel computers. *Meteor. Z.*, **10**, 363–372, doi:10.1127/0941-2948/2001/0010-0363.

——, and T. Franke, 2011: Structure and formation of dust devil–like vortices in the atmospheric boundary layer: A high-resolution numerical study. *J. Geophys. Res.*, **116**, D16120, doi:10.1029/2011JD016010.

Sullivan, P. P., J. C. McWilliams, and C.-H. Moeng, 1996: A grid nesting method for large-eddy simulation of planetary boundary-layer flows. *Bound.-Layer Meteor.*, **80**, 167–202, doi:10.1007/BF00119016.

Tatarskii, V. I., 1961: *Wave Propagation in a Turbulent Medium*. Dover, 285 pp.

Wainwright, C. E., T. A. Bonin, P. B. Chilson, J. A. Gibbs, E. Fedorovich, and R. D. Palmer, 2015: Methods for evaluating the temperature structure-function parameter using unmanned aerial systems and large-eddy simulation. *Bound.-Layer Meteor.*, **155**, 189–208, doi:10.1007/s10546-014-0001-9.

Williamson, J. H., 1980: Low-storage Runge–Kutta schemes. *J. Comput. Phys.*, **35**, 48–56, doi:10.1016/0021-9991(80)90033-9.

Wilson, C. J., and E. Fedorovich, 2012: Direct evaluation of refractive-index structure functions from large-eddy simulation output for atmospheric convective boundary layers. *Acta Geophys.*, **60**, 1474–1492, doi:10.2478/s11600-012-0063-3.

Wyngaard, J. C., 2010: *Turbulence in the Atmosphere*. Cambridge University Press, 393 pp.

——, Y. Izumi, and S. A. Collins Jr., 1971: Behavior of the refractive-index-structure parameter near the ground. *J. Opt. Soc. Amer.*, **61**, 1646–1650, doi:10.1364/JOSA.61.001646.